

pubs.acs.org/Macromolecules Article

Mixed-Polarity Copolymers Based on Ethylene Oxide and Cyclic Carbonate: Insights into Li-Ion Solvation and Conductivity

Peter Bennington, Regina J. Sánchez-Leija, Chuting Deng, Daniel Sharon, Juan J. de Pablo, Shrayesh N. Patel,* and Paul F. Nealey*



Cite This: *Macromolecules* 2023, 56, 4244–4255



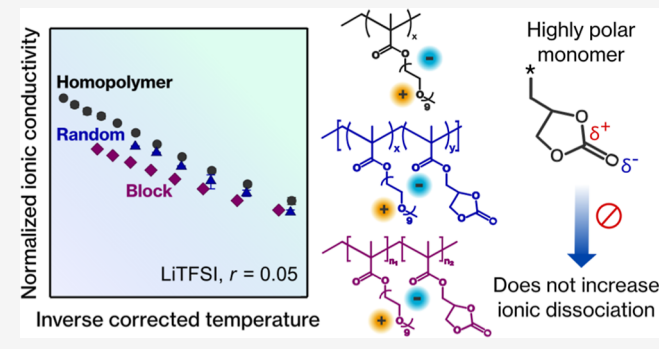
ACCESS I

III Metrics & More

Article Recommendations

s Supporting Information

ABSTRACT: This study investigates the relationship between polarity and ionic conductivity in random and block copolymer electrolytes comprising highly flexible oligo(ethylene oxide) methyl ether methacrylate (OEM) and highly polar but glassy glycerol carbonate methacrylate (GCMA) monomers, blended with either lithium bis(trifluoromethanesulfonyl)imide (LiTFSI) or lithium triflate. Interestingly, the high polarity of GCMA did not significantly enhance ionic dissociation, and the random copolymers (POEM-r-PGCMA) showed similar or lower ionic conductivities than the POEM homopolymer. Further analysis revealed that Li⁺ only interacts with OEM and its counterion, not with GCMA. The less-intermixed and weakly phase-separated



block copolymer (POEM-b-PGCMA) exhibited even lower conductivities than the random copolymer. Our results suggest that Li⁺ solvation occurs only in the POEM-rich phase and that the larger PGCMA regions, depleted of Li⁺, disrupt long-range ion transport. These findings provide valuable insights into the design of polymer electrolytes and how segmental mobility and functional groups with contrasting polarities affect ion transport.

INTRODUCTION

Solid polymer electrolytes (SPEs) continue to attract attention as potential alternatives to conventional liquid electrolytes for next-generation lithium-ion (Li⁺)-based batteries.^{1,2} Poly-(ethylene oxide) (PEO) and polyethers in general have long been leading candidates for this application due to their relatively fast segmental dynamics and their ability to readily solvate Li⁺. However, the practical use of a polyether SPE in a Li⁺ battery requires improvements in several material properties, with insufficient ionic conductivity of PEO at room temperature being the most significant one. In liquid electrolyte systems, high ionic conductivity is commonly achieved by mixing a high-polarity, high-viscosity solvent (such as ethylene carbonate, EC, ε_s = 89.8) with a low-polarity, low-viscosity solvent (such as dimethyl carbonate, DMC, ε_s = 3.1).4-6 These electrolyte mixtures exhibit higher ionic conductivity than that of either solvent alone, owing to the high dielectric constant of EC and the low viscosity of DMC.

Inspired by the success of mixing small-molecule electrolytes, recent work has attempted to apply this concept to SPEs to enhance ionic conductivity. A coarse-grain MD simulation study demonstrated that miscible blends of polymers with contrasting polarities may exhibit greater ionic conductivity than their polymer counterparts. The increased ionic conductivity comes from an increase in charge carrier concentration, since the high-polarity component in blends

promote ionic dissociation. However, an experimental study found that blending PEO with the more polar poly(etheracetal) did not improve the ionic conductivity. In addition, recent work from our group showed that blending PEO with a nonconductive polymer like poly(methyl methacrylate) (PMMA) is detrimental to its conductivity due to the disruption of long-range solvation site connectivity. In blends, the connectivity of the solvation site network was found to depend not only on segmental mixing but also on the specific chemistries of the components, which determine whether and how solvation sites are formed.

Among mixed polymer electrolytes, the polyether-polycarbonate couple is gaining increasing attention. ¹⁰ Both polyethers and polycarbonates can solvate and conduct Li[†], but their conductivities show different dependence on salt concentration and segmental dynamics. ¹¹ Small-molecule analogues of polyether-polycarbonate electrolytes, containing low-viscosity glymes and high-polarity EC, have shown beneficial synergy with a maximum in conductivity at

Received: March 23, 2023 **Revised:** May 9, 2023 **Published:** May 25, 2023





Scheme 1. Synthesis of POEM-r-PGMA Copolymers and Transformation of the Epoxy Groups to Cyclic Carbonate Groups

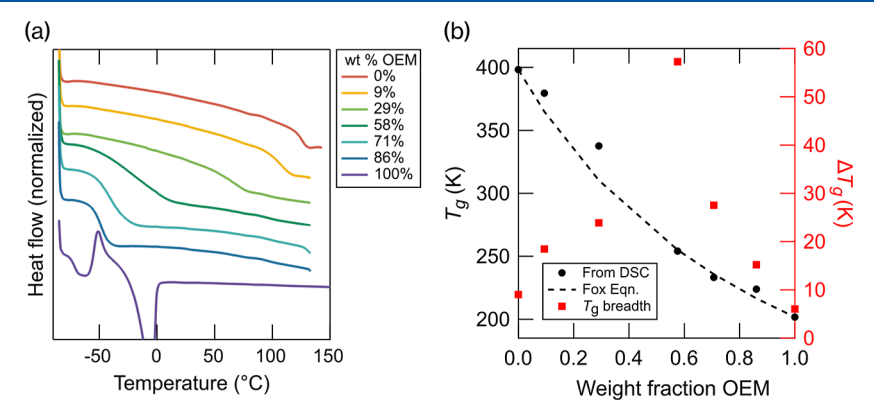


Figure 1. (a) DSC curves of POEM, PGCMA, and POEM-r-PGCMA copolymers. (b) $T_{\rm g}$ of POEM-r-PGCMA copolymers as a function of POEM weight fraction, as determined by DSC. $T_{\rm g}$ values (left axis) were chosen from the midpoint of the transition. $\Delta T_{\rm g}$ (right axis) refers to the breadth of the DSC transition, taken as the difference between the endpoint temperature and onset temperature.

intermediate compositions. 12,13 Although ions in these systems are mainly solvated by the lower-polarity glyme rather than the carbonate, the added carbonate appeared to have a positive effect on the extent of ionic dissociation and hence, conductivity, by increasing the overall dielectric constant. Several studies on copolymers made up of polyethers and linear polycarbonates found that ${\rm Li}^+$ solvation and transport depends on the ether chain length and polymer architecture. The findings indicate that the specific chemistries and chain architectures are critical factors in determining ${\rm Li}^+$ transport in polymer mixtures, highlighting the limitations of relying solely on macroscopic properties such as the dielectric constant and glass-transition temperature $(T_{\rm g})$ as design criteria for polymer electrolyte blends.

To fully explore the potential of mixed polymer electrolytes, it is essential to understand how ionic species interact with functional groups of different polarities. In particular, we focus on polyether-poly(cyclic carbonate) copolymers because the highly polar cyclic carbonate groups introduce significant polarity contrast to the material, and these polymers have been barely explored. In this study, we synthesize and characterize random and block copolymers composed of oligo(ethylene oxide) methyl ether methacrylate (OEM) and glycerol carbonate methacrylate (GCMA) monomers to investigate ionic interactions in copolymers exhibiting high polarity contrast. The POEM homopolymer has a dielectric constant of 10.3, which is close to that of PEO ($\varepsilon_{\rm s} \approx 7$), while cyclic carbonate-substituted polyethers can exhibit much higher dielectric constants of around 62. 16,21

As we varied the content of the highly polar, glassy GCMA in the random copolymer (POEM-r-PGCMA), the difference in ionic conductivities is fully explained by $T_{\rm g}$ effects without any additional contribution from polarity contrast. Raman and IR experiments further support these findings by revealing that ${\rm Li}^+$ are exclusively solvated by the "low-polarity" OEM

monomers. Both the highly dissociated lithium bis-(trifluoromethanesulfonyl)imide (LiTFSI) and the poorly dissociated lithium triflate (LiTf) salts show no change in their degree of dissociation in the presence of the cyclic carbonate, suggesting that high polarity does not necessarily facilitate salt dissociation. The conductivity of LiTFSI and LiTf systems is proportional to the free ion fraction, indicating that Li⁺ transport occurs *via* the same mechanism in both materials. Li⁺ consistently shows exclusive solvation by POEM segments in the block copolymer (POEM-b-PGCMA). The addition of salt is found to make the otherwise weakly phase-separated POEM and PGCMA phases more compatible, as the solvated salts are believed to increase the local dielectric constant near POEM to match that of PGCMA. The ionic conductivity of the block copolymer was lower than that of the random copolymer. The observed trend can be attributed to disrupted long-range ion transport caused by the presence of larger PGCMA-rich domains.

RESULTS AND DISCUSSION

To study the effects of differing monomer polarity in mixed polymer electrolyte systems on ion solvation and transport, we synthesized and characterized a series of random and block copolymers made up of OEM and GCMA monomers. The OEM monomers exhibit fast segmental dynamics, while the glassy GCMA monomers provide high polarity. In this work, each OEM side chain has nine ethylene oxide (EO) repeat units, so the subscript denoting the side-chain length is omitted for clarity.

POEM-r-PGCMA copolymers were synthesized by the twostep reaction shown in Scheme 1. First, OEM and glycidyl methacrylate (GMA) were copolymerized by reversible addition—fragmentation chain transfer (RAFT) polymerization. A series of seven copolymers was synthesized and characterized by size exclusion chromatography (SEC, Figure

S1a) and 1 H NMR (Figure S2) to determine molecular weight and copolymer composition. All copolymers exhibited very similar molecular weight and dispersity, around 10 kg mol⁻¹ and 1.2, respectively (relative to PMMA standards, Figure S1). Figure S1b shows the polymer composition, as determined by 1 H NMR, plotted against the feed composition. Direct fitting to the nonlinear Mayo—Lewis equation gives reactivity ratios r_1 = 0.855 and r_2 = 0.934 (where OEM is monomer 1), indicating that the copolymers should be very close to statistical copolymers. Second, POEM-r-PGMA copolymers were converted to POEM-r-PGCMA by reacting the epoxy groups of the GMA units with CO₂. The reaction was done by dissolving the copolymer in dimethyl formamide along with 10 mol % LiBr (relative to GMA) as a catalyst under 1 atm of CO₂ for 24 h, according to the procedure described by Sakai et al^{22}

POEM and PGMA homopolymers were also prepared by RAFT polymerization, and PGMA was converted to PGCMA in the same manner as the copolymers. Under the aforementioned reaction conditions, both PGMA and POEM-r-PGMA copolymers underwent full conversion of the epoxy groups to cyclic carbonate groups, as evidenced by the absence of proton signals corresponding to the epoxy groups in the 1 H-NMR spectra (Figure S3). Note that GMA monomers can be transformed into GCMA and then polymerized, as previously reported. 23 However, the cyclic carbonate group is susceptible to react with the radical chain end, resulting in branching and crosslinking that can increase both the molecular weight dispersity and T_g . The copolymer composition before and after reaction with CO_2 is listed in Table S1.

The T_g of the POEM-r-PGCMA copolymers, as well as POEM and PGCMA homopolymers, was determined using differential scanning calorimetry (DSC). DSC curves are presented in Figure 1a. The homopolymer POEM exhibits crystallization and melting peaks, but crystallization is completely suppressed by the addition of even 14 wt % GCMA. The $T_{\rm g}$ of each material, plotted in Figure 1b, is taken as the midpoint of the glass transition regime. As seen by the dashed line fit in Figure 1b, the midpoint T_g of POEM-r-PGCMA is reasonably well described by the Fox equation, suggesting that the monomers are intimately and uniformly mixed.²⁴ Importantly, the ether side chains do not exhibit a distinct $T_{\rm g}$ from the rest of the material, as can be seen in miscible blends of PEO and PMMA. The breadth of the glass transition (ΔT_g), however, varies dramatically as a function of the copolymer composition. While POEM and PGCMA homopolymers exhibit only a 5-8 °C window between the onset and end of the glass transition, the glass transition window in the copolymer with 58 wt % OEM extends by nearly 60 °C. This large broadness of the glass transition regime can be interpreted as a broad range of segmental relaxation rates in the material at a fixed temperature. We will discuss later in the text how the dynamic heterogeneity affects ionic conductivity in these copolymers.

To study the ionic conductivity of copolymers with mixed polarity, two copolymers were further examined. Copolymers are referred to as OEM-GC (X-Y) where X and Y refer to the weight percent of OEM and GCMA monomers, respectively. Homopolymer POEM, OEM-GC (86-14), and OEM-GC (58-42) were blended with LiTFSI salt at a ratio of $r = [\text{Li}^+]/[\text{O}] = 0.05$, where [O] is the concentration of ether oxygens and carbonate groups in the system ([O] = [EO] + [OCOO]).

DSC traces for these electrolytes are shown in Figure S4, and the midpoint $T_{\rm g}$ values are reported in Table 1. The increase in

Table 1. Glass-Transition Temperature (T_g) of Polymer Electrolytes

| | | $T_{\rm g}$ (°C) | |
|----------------|-------|------------------|----------------|
| material | neat | r = 0.05, LiTFSI | r = 0.05, LiTf |
| POEM | -71.5 | -56.6 | -55.1 |
| OEM-GC (86-14) | -49.3 | -28.8 | -28.8 |
| OEM-GC (58-42) | -19.1 | -6.8 | -4.4 |
| BCP (50-50) | -55.3 | -29.3 | |

 $T_{\rm g}$ upon the addition of salt is very similar across all materials, and the trend in $\Delta T_{\rm g}$ is preserved. Ionic conductivity of each electrolyte system was then determined by electrochemical impedance spectroscopy (EIS) of thin films cast on interdigitated electrodes (IDEs) as described in our previous studies. Figure 2a shows the ionic conductivity of POEM, OEM-GC (86–14), and OEM-GC (58–42) as a function of temperature. We observed the ionic conductivity to be a function of the polymer composition, with increasing carbonate content resulting in lower conductivity.

To isolate the effects of the copolymer polarity, we normalized the ionic conductivity by two factors: (i) T_{φ} to account for differences in the segmental mobility between materials; and (ii) copolymer composition, to account for differences in the absolute salt content since salt concentration was defined as the molar ratio of Li⁺ to solvating oxygens, which decreases as the carbonate content increases. Similar to the ether oxygen mole fraction introduced in previous studies, 29,30 the solvating oxygen mole fraction, x_0 , is defined as the number of solvating oxygens (ether oxygens in POEM plus the carbonyl oxygens from the carbonate groups in PGCMA) divided by the total number of atoms, excluding hydrogens, in the average repeat unit. The details of these calculations are provided in the Supporting Information. Figure 2b shows the ionic conductivity of POEM, OEM-GC (86-14), and OEM-GC (58-42) with r = 0.05 normalized by the ratio of $x_{O,POEM}/x_O$ plotted as a function of $T-T_g$. When compared at a fixed absolute salt concentration and comparable segmental mobilities, the ionic conductivities of the three materials become highly similar, with a slight decrease observed in OEM-GC (58-42).

Figure 2b reveals that adding a highly polar unit to POEM does not improve the ionic conductivity. On the contrary, the decrease in conductivity shows a positive correlation with the content of the glassy GCMA and can be attributed primarily to differences in the $T_{\rm g}$. While past studies of POEM have found that the bulk-averaged $T_{\rm g}$ does not accurately describe the relaxation rate of the Li⁺ solvating EO units that are most critical to Li⁺ transport, 30,31 the macroscopic description of segmental dynamics is appropriate in the context of this study since side-chain length is held fixed. The similar slope exhibited by these materials in the $T-T_{\rm g}$ plots further indicates that their conductivity is governed by similar dynamics, and that the addition of GCMA primarily contributes to slow down the overall relaxation rates at a fixed temperature.

The difference in the breadth of relaxation rates observed in the DSC measurements appears to have a limited effect on the measured conductivity. The effects of dynamic heterogeneity on Li⁺ transport have been studied previously in the context of POEM of varying side-chain lengths. 30,31 These studies

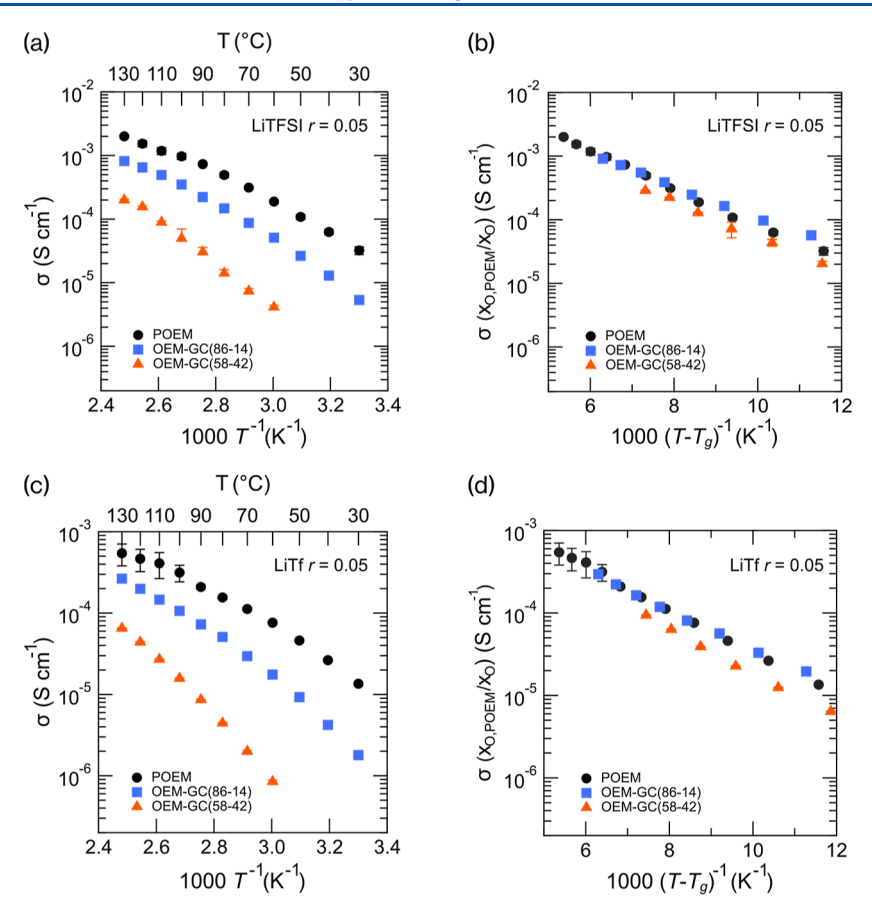


Figure 2. Ionic conductivity of POEM and POEM-r-PGCMA blended with (a) LiTFSI and (c) LiTf. (b,d) Ionic conductivity normalized by the ratio of $x_{O,POEM}/x_O$ plotted as a function of $(T-T_g)^{-1}$. x_O refers to the number of solvating oxygens divided by the total atoms (excluding hydrogen) in the average repeat unit.

indicate that the conductivity is independent of the slow relaxation of the backbones and instead mainly relies on the relaxation of the Li⁺-solvating EO units of the side chains, particularly the mobile side-chain ends. We believe this is also the case for the materials examined here. Li⁺ transport could occur primarily at the more mobile side-chain ends, though the mobilities of these side chains as a whole can be uniformly suppressed by the presence of the glassy GCMA units, the extent of which is quantified by $T_{\rm g}$. While differences in segmental dynamics between materials

explain most conductivity differences at a fixed absolute salt concentration, the residual decrease in conductivity observed in GC-OEM (58-62) likely comes from differences in solvation site density and connectivity. These factors have been highlighted in previous studies as being critical to Li+ transport in linear polyethers, ^{29,32} side-chain polyethers, ³⁰ polyether-polycarbonate copolymers, ¹⁴ and mixed SPEs of PEO and PMMA. Typically, the solvation site density and connectivity relate directly to the mole fraction of EO units, and the dilution of solvation sites due to the presence of GCMA units has been largely accounted for by normalizing the conductivity. In this study, additional effects of such dilution are observed in copolymers with the highest carbonate content, OEM-GC (58-42), as evidenced by their slightly lower normalized conductivities. In mixed SPEs, these second-order effects may relate to an uneven distribution of solvation sites caused by concentration fluctuations of different components. Nonetheless, compared to the detrimental suppression of Li⁺ transport when PMMA is blended with PEO, here the

dilution effect due to GCMA seems to reduce conductivity only slightly. One possible explanation for this observation may be related to the long side-chain architecture of POEM. Unlike linear or short side-chain architectures, the long side chains (nine EO repeat units) of POEM are each fully capable of forming highly mobile solvation sites, independent of any backbone disruption caused by mixing.

In mixed systems where a synergy between polymer polarity and mobility has been observed, the slowed mobility induced by the high-polarity polymer is offset by an increase in salt dissociation, thereby increasing the number of free ions, which is facilitated by the high polarity. 7,20,33 The limited improvement in salt dissociation seen in Figure 2b may simply arise from the highly dissociating nature of LiTFSI in polyethers. At a concentration of r = 0.05, LiTFSI tends to fully dissociate, as observed by Raman spectroscopy.³⁴ Therefore, to corroborate our findings regarding the role of high polarity on salt dissociation in polymer electrolytes, we characterized an additional set of electrolytes consisting of POEM, OEM-GC (86-14), and OEM-GC (58-42), each blended with r = 0.05LiTf. Since LiTf is known to poorly dissociate in polyany increase in salt dissociation due to the presence of GCMA units would be reflected by a significant increase in conductivity. Figure 2c,d indicates that the temperature and composition dependence of conductivity for LiTf systems is identical to that of LiTFSI systems, suggesting again that the presence of GCMA along the backbone barely improves the extent of salt dissociation and instead mainly

affects conductivity by uniformly slowing down the segmental dynamics.

To quantitatively compare how the cyclic carbonate content influences conductivity for the two lithium salts, we present the relative conductivity of the copolymer systems with respect to the POEM counterpart for each salt in Figure 3a. The relative

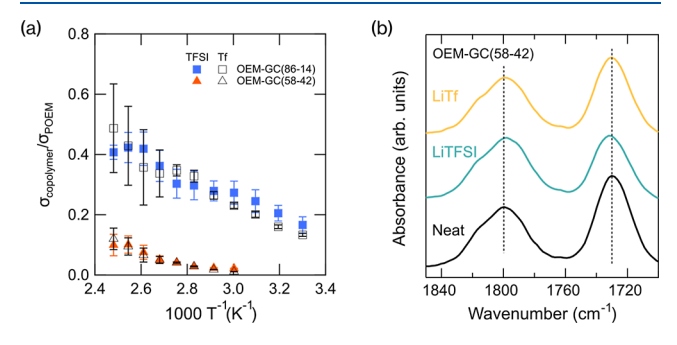


Figure 3. (a) Ionic conductivity of POEM-r-PGCMA normalized by the conductivity of POEM at r = 0.05 with different salts as a function of inverse temperature. (b) FTIR spectra of OEM-GC (58–42) neat (black), r = 0.05 LiTFSI (teal), and r = 0.05 LiTf (yellow).

conductivities depend solely on the cyclic carbonate content because of the increase in $T_{\rm g}$ with increasing content of the glassy monomer. In contrast, the identity of the anion does not affect the relative conductivity, indicating an identical degree of salt dissociation with and without the presence of GCMA. The observed trends in the relative conductivities can be explained by analyzing the FTIR spectra (Figure 3b). In OEM-GC (58–42), the characteristic peaks for the cyclic carbonate group (1800 cm $^{-1}$) and the methacrylate ester (1731 cm $^{-1}$) are entirely unperturbed by the addition of either salt. Any interaction between the cyclic carbonate group and Li $^{+}$ would be evident as a shoulder or a peak at lower wavenumbers. Instead, FTIR spectra reveal that neither the carbonate nor the methacrylate group is involved in solvation, suggesting that Li $^{+}$ is exclusively solvated by ether oxygens.

The free ion fraction in the systems can be more directly assessed by examining the Raman spectra (Figure 4). In LiTFSI copolymer electrolytes, the narrow peak centered around 740 cm⁻¹ is representative of free anions, ^{34,39,40} while the peak near 744 cm⁻¹ corresponds to ion pairs and higher-order aggregates. ⁴¹ Raman spectra can be deconvoluted to determine the amount of free and associated ions by performing peak fitting using two Voigt peaks centered at 740 and 744 cm⁻¹. For all LiTFSI copolymer electrolytes, the peak corresponding to associated ions contributes only 1 % to

the total area of the signal, indicating complete dissociation of the salt (Figure S5). In contrast, spectra of the LiTf copolymer electrolytes show consistently low degree of salt dissociation independent of the carbonate content (Figure S5). For this salt, the extent of ionic dissociation can be estimated based on signals from two characteristic Raman regions, corresponding to the symmetric CF₃ deformation mode (740–770 cm⁻¹) and to the SO₃ symmetric stretch³⁷ (1000–1080 cm⁻¹), see Figure 4b,c. Free ions, ion pairs, and ionic aggregates appear at 753, 757, and 761 cm⁻¹, respectively, for the δ_s (CF₃) region; and at 1033, 1041, and 1051 cm⁻¹, respectively, for the ν_s (SO₃) region.^{37,42} The signals from both regions show significant ion pairing and aggregation in all LiTf copolymer electrolytes. We believe that the presence of cyclic carbonate groups does not affect the degree of dissociation since the position and shape of these peaks appear to remain constant at different carbonate contents.

The free ion fraction in the LiTf electrolytes can be further quantified by performing peak fitting in the δ_s (CF₃) region. While previous studies have used the ν_s (SO₃) region for fitting, the presence of a small peak at approximately 1030 cm⁻¹ arising from the polymer backbone makes quantitative analysis in this region more challenging. In this study, we instead fit the 720-780 cm⁻¹ Raman region because it is completely free of polymer modes. Figure S5 shows peak fitting of these spectra using a linear background and three Voigt functions, from which the free ion fraction was estimated as the area under the 753 cm⁻¹ peak divided by the total fit area. Figure 5a shows full dissociation of LiTFSI salt in all the copolymers and around 25% dissociated LiTf salt. Furthermore, the degree of salt dissociation is constant across the different polymers, with POEM exhibiting a slightly higher fraction of free ions than the copolymers. Figure 5b shows the conductivity of LiTf-containing electrolytes relative to those of their LiTFSI counterparts. It appears that the ratio of conductivities in Figure 5b matches closely to the ratio of free ion fractions shown in Figure 5a. Because the salts only differ in the anion type and are compared at similar segmental mobilities, their difference in conductivity (a ratio of around 0.3) can be primarily attributed to the percentage of mobile, free charge carriers (a ratio of around 0.25). To summarize, quantitative analysis on ionic conductivity and ion solvation environment suggests that the highly polar GCMA units do not facilitate salt dissociation and, instead, reduce conductivity by slowing down the overall segmental dynamics.

Our results reveal rich physical insights regarding the Li⁺ solvation tendency. In these mixed-polarity polymer electrolyte systems, most Li⁺ are fully solvated by EO units instead of the

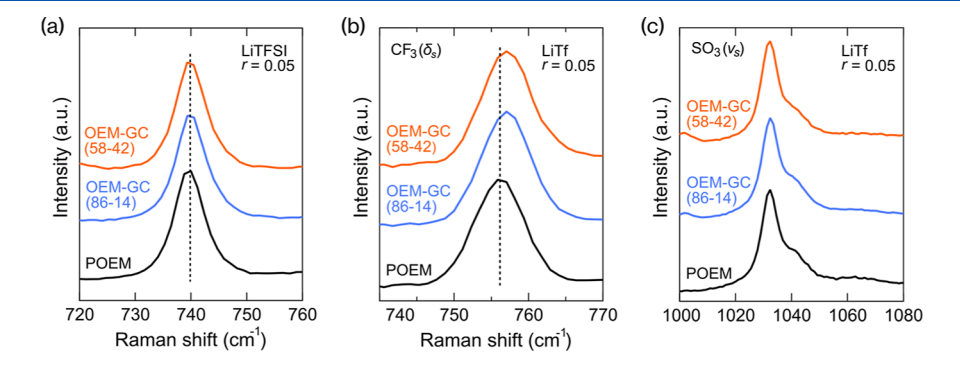
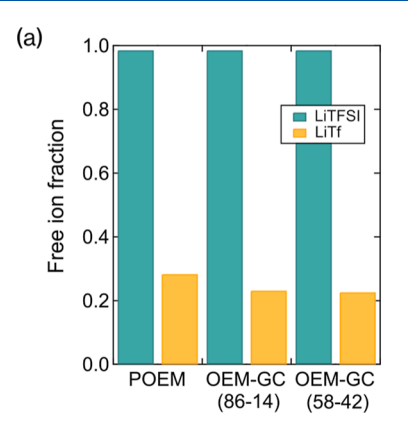


Figure 4. Raman spectra of POEM, OEM-GC (86–14), and OEM-GC (58–42) blended with (a) r = 0.05 LiTFSI and (b,c) r = 0.05 LiTf.



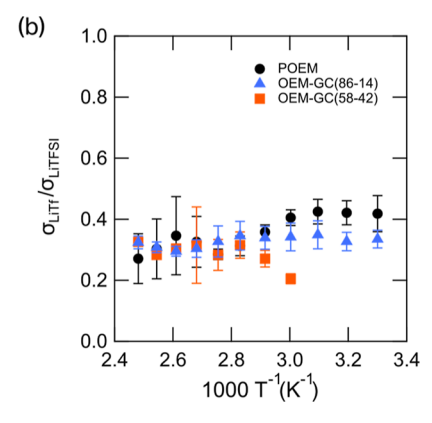


Figure 5. (a) Free ion fraction as determined from peak fitting of Raman data, and (b) ionic conductivity of the LiTf-containing systems divided by that of the corresponding LiTFSI-containing systems as a function of inverse temperature.

cyclic carbonate group, whereas others are partially solvated by the EO units and remain in close contact to the Tf-. Despite its high polarity, the cyclic carbonate groups seem to have lower affinity for Li⁺ than either EO units or the counterions. We hypothesize that the preferential Li⁺ solvation by the ether group arises from the ability of each individual OEM monomer to form a full-fledged solvation site consisting of six ether oxygens.^{30,31} While it appears somewhat unexpected that the solvation tendency in these materials does not correspond to the polarity of the solvating units, previous studies of similar materials have also reported that solvation tendencies depend on the specific material chemistry, in addition to the polarity factor. In a computational study of a series of polyetherpolycarbonate copolymers, Webb et al. found that Li⁺ solvation by the ether groups was generally favorable, and if side-chain ethers were present, Li⁺ was exclusively solvated by those side chains rather than the carbonate groups. 14 Conversely, Morioka et al. experimentally showed that in a linear PEOpolycarbonate, Li+ was actually preferentially solvated by the carbonate groups, and the salt concentration-dependent conductivity and T_{σ} were characteristic of linear poly(ethylene carbonate), not PEO.⁴³ In a different experimental study on polycarbonate-polyether copolymers with varying amounts of linear and cyclic carbonate linkages in the chain, it was found that Li⁺ is preferentially solvated by the cyclic carbonates groups. 16,17 This phenomenon was observed at high salt concentrations, while at low salt concentrations, Li⁺ primarily coordinated with EO units. Moreover, in POEM-r-PGCMA gel polymer electrolytes (swollen with 1:1 EC/DMC solvent), ions were found to be primarily solvated by the cyclic EC solvent, as is typical in polymer-free EC/DMC electrolytes.⁴⁴ The Li⁺ that did interact with the polymer host, however, exclusively interacted with OEM and not GCMA.

To understand the observed solvation tendencies, we need to consider the thermodynamic driven forces that govern ionic dissociation. When a salt dissolves, the enthalpy of the system increases due to the breakup of the ion—ion interactions in the crystal (the lattice energy). This enthalpy increase is balanced out by a decrease in enthalpy from ion—dipole interactions between the ions and the solvent, as well as an increase in entropy when the salt dissolves. In small-molecule systems, an increase in solvent polarity leads to a greater decrease in enthalpy from ion—solvent interaction, which favors dissociation. In polymers, this should also be the case, and more polar polymers should facilitate ion dissociation. However, there is an entropic penalty associated with having more free ions in

polymer electrolytes, as they can act as crosslinking sites and require very specific chain conformations to form solvation sites. 45,46 This specific entropic driving force is characteristic of polymer electrolytes and explains why an increase in contact ion pairs is observed as temperature increases. 45,46 The entropy argument also explains why the ratio of LiTf conductivity to LiTFSI conductivity decreases as temperature increases (Figure 5b). Compared to LiTFSI that remains fully dissociated across all temperatures, the poorly dissociating LiTf may have a slightly increasing fraction of contact ion pairs as temperature increases.

In addition to free ion fraction, the entropic penalty argument also explains the competition between POEM and PGCMA to solvate Li⁺. PGCMA, being highly polar, exhibits a stronger ion-dipole interaction with Li⁺ and larger favorable enthalpy compared to POEM. However, POEM can solvate Li⁺ with minimal entropic penalty, which offsets its relatively enthalpy gain. The entropic penalty of Li+-POEM solvation is minimized since the presence of a solvated Li⁺ hardly perturbs the equilibrium configuration of the nine repeat unit side chain.³¹ Moreover, at these relatively low salt concentrations there are enough POEM side chains to form complete solvation sites with no need for crosslinking. 30,31 Ultimately, in these copolymer systems, POEM, PGCMA, and the counterions compete to solvate Li+ based on their thermodynamic driving forces, and the system reaches its lowest energy configuration when Li⁺ are exclusively solvated or form contact ion pairs in the POEM phase, despite the high dipole moment of the GCMA monomers.

The minimal entropy loss in polyether solvation may also arise from the proximity of solvating units. Since each OEM monomer provides nine EO units covalently bonded along the side chain for Li⁺ solvation, the ether units are inherently closer to each other than carbonate units. In contrast, GCMA monomers only provide one carbonate group, which are randomly distributed along the copolymer backbone. To best illustrate this idea, we can compare the POEM-b-PGCMA block copolymer (BCP) with the POEM-r-PGCMA random copolymer (RCP). Unlike the RCP, GCMA monomers in the BCP will be covalently bonded mostly to other GCMA monomers, and the carbonate groups will be in much closer proximity to each other than in the random configuration. The synthesis of the BCP is described in Scheme S1. First, a PGMA macroCTA was polymerized by RAFT. This living polymer was then purified and used as the RAFT agent for subsequent polymerization of POEM to obtain POEM-b-PGMA, which

was determined to have $M_n = 18.4 \text{ kg mol}^{-1}$, D = 1.29 by SEC (relative to PMMA standards). Finally, POEM-b PGMA was converted to POEM-b-PGCMA by the same CO₂ addition protocol described for the random copolymers (Scheme S2). The resulting polymer was determined to be 50 wt % POEM by 1 H NMR (Figure S6).

We performed DSC measurements to probe segmental dynamics and the degree of mixing in the BCP. DSC curves for the neat and r = 0.05 LiTFSI containing BCP are shown in Figure S7 and the midpoint T_g values are reported in Table 1. In the neat system, only one transition is evident at around -56 °C, which can be attributed to the POEM block, while no signal related to the PGCMA block can be identified. By comparing the DSC curve of the BCP with that of the RCP at similar polymer composition [OEM-GC (58-42)], we find that the absence of DSC signal related to the PGCMA block may not necessarily indicate a fully disordered phase. Compared to the RCP, the BCP shows a significantly lower $T_{\rm g}$ (>30 °C difference in the neat materials) and a much narrower glass transition breadth, both of which suggest that the GCMA and OEM repeat units are much less intimately mixed in the BCP than in the RCP. This difference in local monomer concentration is apparent from small-angle X-ray scattering (SAXS) as well. Figure 6 shows SAXS data for the

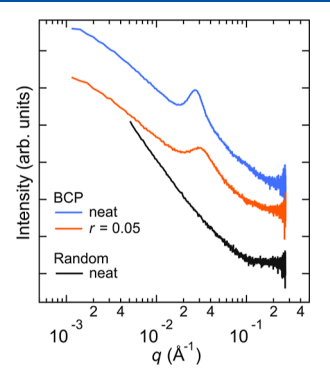


Figure 6. SAXS data from neat OEM-GC (58–42), neat block copolymer, and r = 0.05 LiTFSI blended block copolymer.

neat BCP and OEM-GC (58–42) after annealing at 150 °C. The BCP shows a clear primary scattering peak, indicative of some degree of phase separation, whereas the scattering profile for the RCP is featureless. The real spacing of the primary peak for BCP profile is around 20 nm, which is typical for this material at its molecular weight. The absence of higher order

peaks indicates that the polymer is weakly phase-separated. Overall, the SAXS profiles indicate that the neat BCP is not fully phase-separated, but it exhibits a notable degree of local concentration fluctuations, whereas the RCP is uniformly mixed.

The addition of LiTFSI seems to promote mixing between the two blocks in the BCP. The SAXS profile for the r = 0.05LiTFSI containing BCP is shown in Figure 6. Notably, the primary scattering peak softens and shifts to higher q (lower real spacing), both of which indicate more intimate mixing between the two blocks than in the neat system. The saltdoped BCP still shows some degree of local concentration fluctuations when compared to the RCP. However, the DSC results provide evidence that the salt effectively makes the two blocks more compatible. The addition of Li salt, either LiTFSI or LiTf, to the homopolymer POEM or the RCP has very similar effect on the $T_{\rm g}$ in all cases. However, while adding r=0.05 LiTFSI to OEM-GC (58–42) increases the $T_{\rm g}$ by around 12 °C, the addition of the same amount of salt to the BCP results in a T_g increase of 26 °C. While adding salt to a polymer is well-known to increase the T_g due to an ionic crosslinking effect, in the case of the BČP, the additional increase in $T_{\rm g}$ comes from enhanced mixing between the two blocks, where the glassy PGCMA further slows down the dynamics of the POEM phase.

FTIR spectra can provide insights into the Li⁺ solvation environment and possible reasons for the enhanced mixing in the BCP upon the addition of salt. Figure 7 presents a comparison of FTIR spectra of the BCP and the OEM-GC (58–42) random copolymer. The spectra of the neat materials (Figure 7a) are practically identical in the carbonyl region, suggesting that POEM does not significantly interact with the carbonate or ester moieties of PGCMA in either case. Figure 7b,c shows that the addition of either LiTFSI or LiTf salt does not affect the signal corresponding to the cyclic carbonate groups in each material, demonstrating that the Li salt is localized in the POEM phase regardless of the degree of mixing. Surprisingly, the higher local concentration of PGCMA does not promote Li+ solvation by the carbonate moieties. Even when the cyclic carbonate groups are locally concentrated and available for forming a solvation site, the entropic penalty associated with forming a PGCMA solvation site rather than a POEM solvation site is still too high to be overcome by the already strong ion-dipole interaction between Li+ and PGCMA.

Although the polarity of PGCMA has little influence on the solvation behavior of Li⁺ in the system, the polarity mismatch

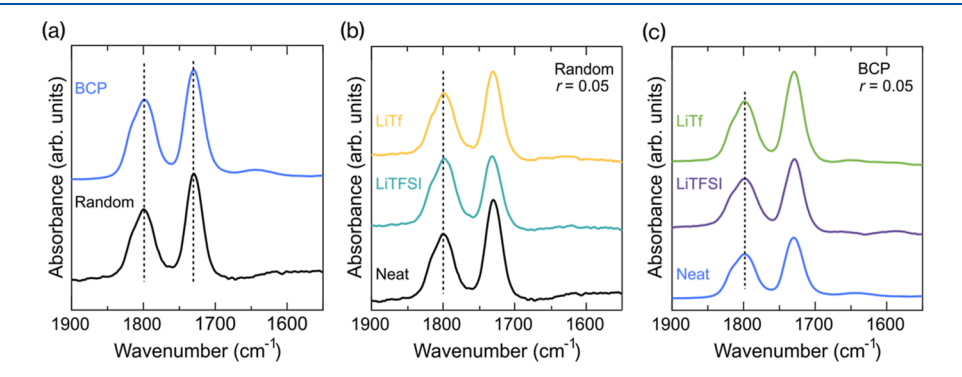
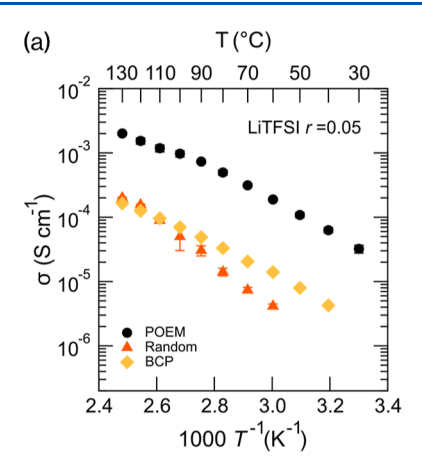


Figure 7. (a) FTIR spectra of neat POEM-r-PGCMA (58–42) and POEM-b-PGCMA (50–50). FTIR spectra of (b) random copolymer and (c) block copolymer with r = 0.05 LiTFSI and LiTf.



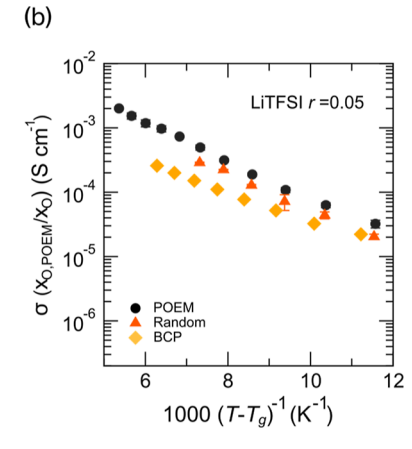


Figure 8. (a) Ionic conductivity of POEM, OEM-GC (58–42), and BCP (50–50) as a function of T^{-1} . (b) Ionic conductivity normalized by the ratio of $x_{O,POEM}/x_O$ plotted as a function of $(T-T_g)^{-1}$.

between the two blocks does appear to describe the phase behavior observed. The phase separation in the neat POEM-b-PGCMA, even though weak, can be partially understood from the different polarities and dielectric constants of the two blocks. 47 As salt is added to the material, it is preferentially solvated and localized in the low-polarity POEM phase. This counterintuitive fact can be explained under the polymerspecific thermodynamic considerations already mentioned. The ion solvation and salt localization are driven by molecular-level factors and the specific chemical nature of the polyether side chains, while the effects of added salt on the material phase behavior can be explained by macroscopic phenomena, such as the dielectric constant. The localization of salt in the low-polarity material increases the effective dielectric constant of that phase, thereby decreasing the contrast with the high-polarity, salt-free block. This is in contrast to what has been recently observed in high-polarity contrast block copolymers electrolytes consisting of poly(ally glycidyl ether), a low-polarity/low-viscosity component, and poly-(cyanoethyl glycidyl ether), a high-polarity component. In this case, the high-polarity phase has a strong preference for the salt and does primarily solvate Li⁺ at low salt concentrations, which increases the polarity contrast and in turn the immiscibility between the blocks.

Finally, we measured the ionic conductivity of the BCP r =0.05 LiTFSI system. Figure 8a shows the conductivity of the BCP system after annealing at 150 °C for 2 h compared to the homopolymer POEM and the OEM-GC (58-42) random copolymer electrolyte. The BCP exhibits higher conductivity than the RCP at low temperatures, but it has a weaker temperature dependence due to its lower $T_{\rm g}$. At around 110 °C, the conductivity of the RCP reaches and then slightly exceeds that of the BCP. After correcting for differences in T_{σ} (Figure 8b), however, the RCP shows a higher conductivity at nearly all reduced temperatures. Moreover, while the RCP and homopolymer share a common slope, suggesting a similar activation energy limiting the conductivity, the BCP exhibits a qualitatively different behavior. This may be partly because the phase behavior of the BCP is temperature-dependent. Another factor likely lies in the formation and percolation of solvation sites.

The results show that the RCP, the copolymer with a higher degree of intimate mixing, exhibits a higher conductivity than the weakly phase-separated BCP. This finding appears to contradict our previous results and those of others. We have

hypothesized previously that the greater extent of interfacial mixing present in low salt concentration block copolymer PS-PEO explains the lower normalized conductivity.²⁸ Similarly, our recent work found that miscible blends of PEO/PMMA have a higher conductivity than the compositionally identical PEO-PMMA block copolymers. We attributed this fact to a greater local concentration of PEO in the less-mixed blends that led to greater percolation of solvation sites at the 5-10 Å length scale that allows for long-range Li⁺ transport. A key difference between those studies and the present work seems to lie in the use of linear rather than side-chain polyethers. In the case of linear PEO, solvation sites are formed by adjacent EO units along the backbone. These solvation sites may be more susceptible to disruption or disconnection by nonsolvating groups like PS or PMMA groups, in contrast to the side-chain solvation sites in POEM, which are less affected. Additionally, the disruption of solvation sites along the backbone tends to suppress the intrachain hopping mechanism that is common in linear PEO, but largely absent in side-chain POEM systems.³¹ As Li⁺ solvation and transport in POEM do not rely on the backbone, the detrimental effects caused by the mixing with nonsolvating components are limited. This apparent difference in how mixing affects Li⁺ transport in linear and side-chain polyethers provides valuable insights for the study of block copolymer electrolytes, where the transport through the interfacial region is highly coupled to the degree of interfacial mixing. ^{28,48–50} These questions merit further investigation, particularly using atomistic MD simulations similar to those recently employed to investigate ion hopping between solvation sites.

CONCLUSIONS

In this study, we elucidated the ion solvation and transport behavior of copolymers consisting of a side-chain polyether (POEM) and a poly(cyclic carbonate) (PGCMA). Although the cyclic carbonate moiety is significantly more polar than the ether oxygens of POEM, FTIR data and ionic conductivity results suggest that Li⁺ are exclusively solvated and transported by POEM. The increased overall polarity of the polymer does not enhance the conductivity. Instead, the conductivity of the random copolymer is solely determined by the mole fraction of EO units in the system and the bulk-averaged dynamics, as evidenced by the midpoint $T_{\rm g}$ value. Furthermore, we demonstrated that our findings are also valid when a poorly dissociating LiTf salt is added to the system. Raman data for

both LiTFSI- and LiTf-containing polymer electrolytes confirm that the presence of highly polar carbonate moieties does not increase the degree of ionic dissociation, regardless of the dissociating nature of the salt. In the partially dissociated LiTf systems, our results indicate that the thermodynamically favorable state consists of a high fraction of contact ion pairs with Li⁺ partially solvated by POEM side chains. The observed tendency for solvation in these polymer systems is driven by entropic considerations for ion dissociation. These findings suggest that blending or mixing a highly polar component with an ether-based polymer may not be an effective strategy for improving ionic conductivity unless specific material chemistries for Li⁺ solvation are considered.

Finally, the same preference for polyether solvation was found in the block copolymer, despite the high local concentration of cyclic carbonate groups available to form solvation sites. This preference for the salt to reside in the lower-polarity POEM phase decreases the polarity contrast with the PGCMA phase, and SAXS data indicate that the addition of salt lowers the effective Flory-Huggins interaction parameter of the material. The block copolymer exhibited reduced conductivity and qualitatively different temperature dependency compared to the homopolymer and random copolymer systems. The reduced conductivity of the block copolymer can be attributed to the disruption of long-range percolated solvation site networks due to clustering of the POEM units. Opposite to trends observed in mixed polymer electrolytes based on linear PEO, the side-chain POEM-based copolymers examined here show reduced conductivity with increasing contrast in the local concentration (less mixing). The relationship between the degree of mixing and ion transport may be fundamentally different in side-chain polyethers than in linear polyether electrolytes. The reason behind this lies in the fact that the nine EO unit side chain in POEM can form full solvation sites, whereas the formation of solvation sites in PEO requires a continuous and uninterrupted backbone. This also suggests that with a moderate degree of local mixing, the percolation of solvation site network is likely still preserved in the random copolymer. The discussion presented here on the relationship between degree of mixing and Li⁺ transport can perhaps be extended to other polymer electrolyte systems containing side-chain ethers, such as those found in phase-separated POEM-based block copolymer electrolytes, to better understand and design mixed, multifunctional polymer electrolytes.

■ EXPERIMENTAL SECTION

Materials. Acetonitrile (99.8%, anhydrous), toluene, dimethylformamide (DMF), tetrahydrofuran (THF), methanol, diethyl ether, LiTFSI (battery grade, >99.95% trace metal basis) LiTf (99.995% trace metals basis), 2-cyano-2-propyl benzodithioate (CPBD), azobisisobutyronitrile (AIBN), deuterated dimethyl sulfoxide (DMSO- d_6), and monomers were purchased from Sigma-Aldrich. Oligo(ethylene oxide) methyl ether methacrylate (OEM, $M_n = 500$ g mol $^{-1}$) and glycidyl methacrylate (GMA) were purified before use to remove inhibitors by passing through a column of basic alumina. LiTFSI was dried under vacuum at 120 °C for 48 h. Homopolymer POEM was synthesized and purified according to our previous work. Polymers and salts were stored in an argon glovebox after the drying processes. AIBN was recrystallized in ethanol before use.

Polymer Synthesis. Synthesis of POEM-r-PGMA Copolymers. POEM-r-PGMA random copolymers were synthesized by RAFT polymerization according to Scheme 1. Reaction mixtures consisting of 5 g of total monomer, 9.1 g (9.6 mL) of DMF, 55.3 mg of CPBD,

and 4.1 mg of AIBN were stirred and sparged with dry nitrogen for 20 min. Mass fractions of OEM in the feed and final product are listed in Table S1. Reactions proceeded for 7 h at 70 $^{\circ}$ C followed by quenching the vessel in an ice bath. The crude products were purified by evaporating DMF, redissolving in THF, and precipitating the mixtures into excess hexanes. The resulting polymers were redissolved in THF and precipitated into hexanes twice more and dried overnight at 50 $^{\circ}$ C to remove residual solvent.

Synthesis of POEM-b-PGMA Copolymers. POEM-b-PGMA block copolymers were synthesized by RAFT polymerization according to Scheme S1. First, PGMA macroCTA was prepared by RAFT polymerization of GMA. 5 g of GMA, 9.3 g (9.8 mL) of DMF, 55.3 mg of CPBD, and 4.1 mg of AIBN were stirred and sparged with dry nitrogen for 20 min. The reaction vessel was placed in an oil bath at 70 °C for 7.5 h, followed by quenching in an ice bath. The crude product was purified by precipitating the mixture into excess methanol, followed by redissolution in THF and precipitated into methanol twice more. The resulting polymer was dried overnight at 50 °C to remove residual solvent. PGMA was then used as CTA for subsequent polymerization of the POEM block. 1.5 g of OEM, 1.0 g of PGMA macroCTA, 2.5 mg of AIBN, and 2.4 g of THF (2.7 mL) were stirred to combine in a round-bottom flask and sparged with dry nitrogen. The flask was placed in an oil bath at 70 °C for 6 h before quenching in an ice bath. The crude mixture was precipitated into excess hexanes, followed by redissolution in THF and precipitation in hexanes twice more. The resulting polymer was dried at 50 °C under vacuum overnight.

Transformation of GMA Units to GCMA Units. The epoxy groups of GMA were converted to cyclic carbonate groups by the addition of CO₂. A similar process was used for all random and block copolymers. Polymers were dissolved in DMF (0.2 M) along with 10 mol % LiBr (relative to the GMA units) as a catalyst. CO₂ was bubbled through the reaction mixture for a couple of minutes and then the reaction mixture was heated to 100 °C for 24 h while keeping a CO₂ atmosphere. After the reaction, the polymer solutions were concentrated by evaporating DMF and then precipitated into excess methanol (random copolymers 1 and 2, Table S1) or cold diethyl ether (block and random copolymers 3–5, Table S1), or dialyzed against methanol overnight (random copolymers 6 and 7, Table S1) to recover the product and remove the catalyst. The resulting copolymers were filtered, washed three times using methanol or diethyl ether and finally dried under vacuum overnight at 50 °C.

Polymer Electrolyte Solution Preparation. Polymer solutions were prepared inside of an argon glovebox by dissolving polymer in either pure acetonitrile or a mixture of acetonitrile and toluene (50/50 v/v). Solutions were heated to 50 °C to help facilitate dissolution of the polymer and then were left stirring overnight. LiTFSI solutions in acetonitrile were prepared in the same manner. Polymer electrolyte solutions were prepared by blending polymer and salt solutions at the corresponding volumetric ratio to obtain a ratio of r = 0.05 = [LiTFSI]/[EO].

Polymer Characterization. Size Exclusion Chromatography. SEC measurements were conducted on a Tosoh EcoSEC system with DMF + 0.01 M LiBr as eluent at a flow rate of 1 mL/min. Separation was achieved using two Tosoh SuperAW columns in series (3000 and 4000) at 50 °C. Molecular weight and dispersity were determined by comparison with PMMA standards.

Proton Nuclear Magnetic Resonance (1H NMR). Chemical structural information of the polymers was obtained using 1H NMR in DMSO- d_6 . Data were acquired on a 400 MHz Bruker Avance III HD nanobay spectrometer equipped with an iProbe SmartProbe, using Topspin 2.1. Copolymer composition was determined by comparing the peak integrals at $\delta = 4.03$ ppm (2H, $-C(O)-O-CH_2-$) of POEM units to those at $\delta = 2.80$ and 2.66 ppm (2H, $-CH_2-CH(OCH_2)$) of the epoxy groups of PGMA. The composition of the POEM-r-PGMA copolymers is reported in Table S1. Complete conversion of the epoxide group to cyclic carbonate was confirmed by complete disappearance of peaks at $\delta = 3.20$ ppm (1H, $-CH_2-CH(OCH_2)$) and $\delta = 2.80$ and 2.66 ppm (2H,

 $-\mathrm{CH_2-CH(OCH_2)})$ corresponding to protons in the epoxide groups of PGMA.

Differential Scanning Calorimetry. Calorimetric glass-transition temperatures $(T_{\rm g})$ of neat polymers and copolymer electrolytes were determined by DSC using a TA Instruments Discovery 2500 DSC. Sample pans were prepared inside an argon glovebox by drop-casting solutions, heating at 65 °C until dry, and repeating until 5–10 mg of material were collected in the pan. The pans were then hermetically sealed before removing from the glovebox to avoid any water adsorption before DSC measurement. Samples were conditioned at 135 °C followed by three cycles of cooling to -85 °C and heating to 135 °C at a scan rate of 10 °C/min. $T_{\rm g}$ midpoint and breadth values were taken from the third heating curve.

Fourier Transform Infrared Spectroscopy. Samples for FTIR measurements were prepared on Au-coated Si substrates by spin-coating. Samples were prepared inside of a glovebox, annealed at 150 °C for 15 min, and then sealed immediately before measurement to minimize water absorption. Measurements were performed using a Shimadzu IRTracer-100 spectrometer using a germanium prism for attenuated total reflection at ambient temperature from 400 to 4000 cm⁻¹ at a resolution of 4 cm⁻¹.

Raman Spectroscopy. Raman samples were prepared by drop-casting films on Au-coated Si substrates inside of an argon glovebox. Films were dried and then annealed at 150 °C for 15 min inside of the glovebox and then sealed until measurement. Raman experiments were performed using a Horiba LabRAM HR Evolution NIR confocal Raman microscope. Raman spectra were collected with a 100x objective and a 633 nm wavelength laser.

Small-Angle X-ray Scattering. SAXS measurements were performed using the SAXSLAB GANESHA instrument at the University of Chicago X-ray Facility. Prior the experiments, dry block copolymer samples were annealed in bulk under vacuum at 150 °C for 20 h and then slowly cooled down to ambient temperature to favor self-assembly. Data were collected at ambient temperature for 30 min.

Electrochemical Impedance Spectroscopy. Polymer electrolyte conductivity was determined by EIS of thin films on IDEs as described previously. 28 IDEs were designed with N = 160 electrodes, l= 1 mm of electrode overlap, w = 2 μ m electrode width, and d = 8 μ m interelectrode distance. IDEs were then coated with 0.8 nm of SiO₂ by plasma-assisted atomic layer deposition to inhibit dewetting of the polymer films. Polymer electrolyte thin films were cast onto the IDEs by spin-coating at 4000 rpm inside of an argon glovebox, followed by drying on a hot plate at 70 °C before EIS measurements. Block copolymer films were further annealed at 150 °C for 2 h before measurement. Polymer film height (h) was determined by casting an identical film on a Si wafer and performing ellipsometry (J.A. Woollam alpha-SE ellipsometer). IDEs were placed on a custom heating stage in the glovebox and connected to a Gamry 600+ potentiostat by tungsten probe tips. Potentiostatic EIS was performed with an applied amplitude of 100 mV over a frequency range of 1 MHz to 1 Hz. EIS data were fit to an appropriate equivalent circuit that models the physical process of thin film-IDE systems using Gamry E-chem Analyst software, and the resulting film resistance (R_i) was used to find the conductivity (σ) by the equation below.² conductivity data are reported as the average of three samples, with error bars representing the standard deviation.

$$\sigma = \frac{d}{R_{\rm f}(N-1)lh}$$

ASSOCIATED CONTENT

Supporting Information

The Supporting Information is available free of charge at https://pubs.acs.org/doi/10.1021/acs.macromol.3c00540.

SEC traces, nonlinear Mayo—Lewis equation fit, ¹H NMR spectra, composition of random copolymers, DSC traces, synthesis schemes, Raman spectra fits, solvating

oxygen mole fraction calculation, and normalization of the ionic conductivity (PDF)

AUTHOR INFORMATION

Corresponding Authors

Shrayesh N. Patel — Pritzker School of Molecular Engineering, University of Chicago, Chicago, Illinois 60637, United States; orcid.org/0000-0003-3657-827X; Email: shrayesh@uchicago.edu

Paul F. Nealey — Pritzker School of Molecular Engineering, University of Chicago, Chicago, Illinois 60637, United States; Materials Science Division, Argonne National Laboratory, Lemont, Illinois 60439, United States; ○ orcid.org/0000-0003-3889-142X; Email: nealey@uchicago.edu

Authors

Peter Bennington — Pritzker School of Molecular Engineering, University of Chicago, Chicago, Illinois 60637, United States; orcid.org/0000-0002-0501-1441

Regina J. Sánchez-Leija — Pritzker School of Molecular Engineering, University of Chicago, Chicago, Illinois 60637, United States; Materials Science Division, Argonne National Laboratory, Lemont, Illinois 60439, United States

Chuting Deng — Pritzker School of Molecular Engineering, University of Chicago, Chicago, Illinois 60637, United States; occid.org/0000-0002-0416-178X

Daniel Sharon — Institute of Chemistry, The Hebrew University of Jerusalem, Jerusalem 91904, Israel; orcid.org/0000-0002-3385-1536

Juan J. de Pablo — Pritzker School of Molecular Engineering, University of Chicago, Chicago, Illinois 60637, United States; Materials Science Division, Argonne National Laboratory, Lemont, Illinois 60439, United States; ◎ orcid.org/0000-0002-3526-516X

Complete contact information is available at: https://pubs.acs.org/10.1021/acs.macromol.3c00540

Notes

The authors declare no competing financial interest.

ACKNOWLEDGMENTS

We gratefully acknowledge financial support by the U. S. Department of Energy (DOE), Office of Science, Basic Energy Sciences, Materials Science and Engineering Division. We also acknowledge the Soft Matter Characterization Facility of the University of Chicago where SEC, DSC, and FTIR experiments were performed. This work made use of the shared facilities at the University of Chicago Materials Research Science and Engineering Center, supported by National Science Foundation under award number DMR-2011854 (Raman experiments).

REFERENCES

- (1) Hallinan, D. T.; Balsara, N. P. Polymer Electrolytes. Annu. Rev. Mater. Res. 2013, 43, 503-525.
- (2) Wang, H.; Sheng, L.; Yasin, G.; Wang, L.; Xu, H.; He, X. Reviewing the Current Status and Development of Polymer Electrolytes for Solid-State Lithium Batteries. *Energy Storage Mater.* **2020**, 33, 188–215.
- (3) Xue, Z.; He, D.; Xie, X. Poly(Ethylene Oxide)-Based Electrolytes for Lithium-Ion Batteries. *J. Mater. Chem. A* **2015**, *3*, 19218–19253.
- (4) Xu, K. Nonaqueous Liquid Electrolytes for Lithium-Based Rechargeable Batteries. Chem. Rev. 2004, 104, 4303-4418.

- (5) Zhu, C.; Pedretti, B. J.; Kuehster, L.; Ganesan, V.; Sanoja, G. E.; Lynd, N. A. Ionic Conductivity, Salt Partitioning, and Phase Separation in High-Dielectric Contrast Polyether Blends and Block Polymer Electrolytes. *Macromolecules* **2023**, *56*, 1086–1096.
- (6) Gao, K. W.; Loo, W. S.; Snyder, R. L.; Abel, B. A.; Choo, Y.; Lee, A.; Teixeira, S. C. M.; Garetz, B. A.; Coates, G. W.; Balsara, N. P. Miscible Polyether/Poly(Ether–Acetal) Electrolyte Blends. *Macromolecules* **2020**, *53*, 5728–5739.
- (7) Dahbi, M.; Ghamouss, F.; Tran-Van, F.; Lemordant, D.; Anouti, M. Comparative Study of EC/DMC LiTFSI and LiPF6 Electrolytes for Electrochemical Storage. *J. Power Sources* **2011**, *196*, 9743–9750.
- (8) Wheatle, B. K.; Lynd, N. A.; Ganesan, V. Effect of Host Incompatibility and Polarity Contrast on Ion Transport in Ternary Polymer-Polymer-Salt Blend Electrolytes. *Macromolecules* **2020**, *53*, 875–884.
- (9) Sharon, D.; Deng, C.; Bennington, P.; Webb, M. A.; Patel, S. N.; de Pablo, J. J.; Nealey, P. F. Critical Percolation Threshold for Solvation-Site Connectivity in Polymer Electrolyte Mixtures. *Macromolecules* **2022**, *55*, 7212–7221.
- (10) Zhao, Y.; Bai, Y.; Li, W.; An, M.; Bai, Y.; Chen, G. Design Strategies for Polymer Electrolytes with Ether and Carbonate Groups for Solid-State Lithium Metal Batteries. *Chem. Mater.* **2020**, 32, 6811–6830.
- (11) Kimura, K.; Yajima, M.; Tominaga, Y. A Highly-Concentrated Poly(Ethylene Carbonate)-Based Electrolyte for All-Solid-State Li Battery Working at Room Temperature. *Electrochem. Commun.* **2016**, 66, 46–48.
- (12) Tobishima, S.; Morimoto, H.; Aoki, M.; Saito, Y.; Inose, T.; Fukumoto, T.; Kuryu, T. Glyme-Based Nonaqueous Electrolytes for Rechargeable Lithium Cells. *Electrochim. Acta* **2004**, *49*, 979–987.
- (13) Geoffroy, I.; Willmann, P.; Mesfar, K.; Carré, B.; Lemordant, D. Electrolytic Characteristics of Ethylene Carbonate—Diglyme-Based Electrolytes for Lithium Batteries. *Electrochim. Acta* **2000**, *45*, 2019—2027
- (14) Webb, M. A.; Jung, Y.; Pesko, D. M.; Savoie, B. M.; Yamamoto, U.; Coates, G. W.; Balsara, N. P.; Wang, Z. G.; Miller, T. F. Systematic Computational and Experimental Investigation of Lithium-Ion Transport Mechanisms in Polyester-Based Polymer Electrolytes. *ACS Cent. Sci.* **2015**, *1*, 198–205.
- (15) Morioka, T.; Ota, K.; Tominaga, Y. Effect of Oxyethylene Side Chains on Ion-Conductive Properties of Polycarbonate-Based Electrolytes. *Polymer* **2016**, *84*, 21–26.
- (16) You, D.; Hu, W.; Song, L.; Wei, W.; Xiong, H. High-Energy Metallic Lithium Batteries Enabled by Polymer-in-Salt Electrolytes of Cyclic Carbonate Substituted Polyethers. *ACS Appl. Polym. Mater.* **2022**, *4*, 8584–8593.
- (17) Ouhib, F.; Meabe, L.; Mahmoud, A.; Grignard, B.; Thomassin, J. M.; Boschini, F.; Zhu, H.; Forsyth, M.; Mecerreyes, D.; Detrembleur, C. Influence of the Cyclic versus Linear Carbonate Segments in the Properties and Performance of CO2-Sourced Polymer Electrolytes for Lithium Batteries. ACS Appl. Polym. Mater. 2020, 2, 922–931.
- (18) Huang, B.; Lai, P.; Hua, H.; Li, R.; Shen, X.; Yang, X.; Zhang, P.; Zhao, J. A Copolyether with Pendant Cyclic Carbonate Segment for PEO-Based Solid Polymer Electrolyte. *J. Power Sources* **2023**, *570*, 233049.
- (19) Bartels, J.; Wang, J. H. H.; Chen, Q.; Runt, J.; Colby, R. H. Segmental Dynamics of Ethylene Oxide-Containing Polymers with Diverse Backbone Chemistries. *Macromolecules* **2016**, *49*, 1903–1910.
- (20) Wheatle, B. K.; Keith, J. R.; Mogurampelly, S.; Lynd, N. A.; Ganesan, V. Influence of Dielectric Constant on Ionic Transport in Polyether-Based Electrolytes. *ACS Macro Lett.* **2017**, *6*, 1362–1367.
- (21) Choi, U. H.; Liang, S.; Chen, Q.; Runt, J.; Colby, R. H. Segmental Dynamics and Dielectric Constant of Polysiloxane Polar Copolymers as Plasticizers for Polymer Electrolytes. *ACS Appl. Mater. Interfaces* **2016**, *8*, 3215–3225.
- (22) Sakai, T.; Kihara, N.; Endo, T. Polymer Reaction of Epoxide and Carbon Dioxide. Incorporation of Carbon Dioxide into Epoxide Polymers. *Macromolecules* **1995**, 28, 4701–4706.

- (23) Camara, F.; Caillol, S.; Boutevin, B. Free Radical Polymerization Study of Glycerin Carbonate Methacrylate for the Synthesis of Cyclic Carbonate Functionalized Polymers. *Eur. Polym. J.* **2014**, *61*, 133–144.
- (24) Schneider, H. A. The Meaning of the Glass Temperature of Random Copolymers and Miscible Polymer Blends. *J. Therm. Anal. Calorim.* **1999**, *56*, 983–989.
- (25) Lodge, T. P.; McLeish, T. C. B. Self-Concentrations and Effective Glass Transition Temperatures in Polymer Blends. *Macromolecules* **2000**, *33*, 5278–5284.
- (26) Lodge, T. P.; Wood, E. R.; Haley, J. C. Two Calorimetric Glass Transitions Do Not Necessarily Indicate Immiscibility: The Case of PEO/PMMA. *J. Polym. Sci. B Polym. Phys.* **2006**, 44, 756–763.
- (27) Sharon, D.; Bennington, P.; Liu, C.; Kambe, Y.; Dong, B. X.; Burnett, V. F.; Dolejsi, M.; Grocke, G.; Patel, S. N.; Nealey, P. F. Interrogation of Electrochemical Properties of Polymer Electrolyte Thin Films with Interdigitated Electrodes. *J. Electrochem. Soc.* **2018**, *165*, H1028–H1039.
- (28) Sharon, D.; Bennington, P.; Dolejsi, M.; Webb, M. A.; Dong, B. X.; de Pablo, J. J.; Nealey, P. F.; Patel, S. N. Intrinsic Ion Transport Properties of Block Copolymer Electrolytes. *ACS Nano* **2020**, *14*, 8902–8914.
- (29) Pesko, D. M.; Webb, M. A.; Jung, Y.; Zheng, Q.; Miller, T. F.; Coates, G. W.; Balsara, N. P. Universal Relationship between Conductivity and Solvation-Site Connectivity in Ether-Based Polymer Electrolytes. *Macromolecules* **2016**, *49*, 5244–5255.
- (30) Bennington, P.; Deng, C.; Sharon, D.; Webb, M. A.; de Pablo, J. J.; Nealey, P. F.; Patel, S. N. Role of Solvation Site Segmental Dynamics on Ion Transport in Ethylene-Oxide Based Side-Chain Polymer Electrolytes. *J. Mater. Chem. A* **2021**, *9*, 9937–9951.
- (31) Deng, C.; Webb, M. A.; Bennington, P.; Sharon, D.; Nealey, P. F.; Patel, S. N.; de Pablo, J. J. Role of Molecular Architecture on Ion Transport in Ethylene Oxide-Based Polymer Electrolytes. *Macromolecules* **2021**, *54*, 2266–2276.
- (32) Webb, M. A.; Savoie, B. M.; Wang, Z. G.; Miller III, T. F. Chemically Specific Dynamic Bond Percolation Model for Ion Transport in Polymer Electrolytes. *Macromolecules* **2015**, *48*, 7346–7358.
- (33) Wheatle, B. K.; Lynd, N. A.; Ganesan, V. Effect of Polymer Polarity on Ion Transport: A Competition between Ion Aggregation and Polymer Segmental Dynamics. ACS Macro Lett. 2018, 7, 1149—1154
- (34) Sharon, D.; Bennington, P.; Webb, M. A.; Deng, C.; de Pablo, J. J.; Patel, S. N.; Nealey, P. F. Molecular Level Differences in Ionic Solvation and Transport Behavior in Ethylene Oxide-Based Homopolymer and Block Copolymer Electrolytes. *J. Am. Chem. Soc.* **2021**, *143*, 3180–3190.
- (35) Torell, L. M.; Jacobsson, P.; Petersen, G. A Raman Study of Ion Solvation and Association in Polymer Electrolytes. *Polym. Adv. Technol.* **1993**, *4*, 152–163.
- (36) Huang, W.; Frech, R. Raman Spectra of PPO-Salt Complexes: Mixed Cations and Mixed Anions. *Solid State Ionics* **1992**, *53–56*, 1095–1101.
- (37) Huang, W.; Frech, R. Dependence of Ionic Association on Polymer Chain Length in Poly(Ethylene Oxide)-Lithium Triflate Complexes. *Polymer* 1994, 35, 235–242.
- (38) Kimura, K.; Motomatsu, J.; Tominaga, Y. Correlation between Solvation Structure and Ion-Conductive Behavior of Concentrated Poly(Ethylene Carbonate)-Based Electrolytes. *J. Phys. Chem. C* **2016**, 120, 12385–12391.
- (39) Rey, I.; Lassègues, J. C.; Grondin, J.; Servant, L. Infrared and Raman Study of the PEO-LiTFSI Polymer Electrolyte. *Electrochim. Acta* 1998, 43, 1505–1510.
- (40) Brouillette, D.; Irish, D. E.; Taylor, N. J.; Perron, G.; Odziemkowski, M.; Desnoyers, J. E. Stable Solvates in Solution of Lithium Bis(Trifluoromethylsulfone)Imide in Glymes and Other Aprotic Solvents: Phase Diagrams, Crystallography and Raman Spectroscopy. *Phys. Chem. Chem. Phys.* **2002**, *4*, 6063–6071.

- (41) Aguilera, L.; Xiong, S.; Scheers, J.; Matic, A. A Structural Study of LiTFSI—Tetraglyme Mixtures: From Diluted Solutions to Solvated Ionic Liquids. *J. Mol. Liq.* **2015**, *210*, 238–242.
- (42) York, S.; Frech, R.; Snow, A.; Glatzhofer, D. A Comparative Vibrational Spectroscopic Study of Lithium Triflate and Sodium Triflate in Linear Poly(Ethylenimine). *Electrochim. Acta* **2001**, *46*, 1533–1537
- (43) Morioka, T.; Nakano, K.; Tominaga, Y. Ion-Conductive Properties of a Polymer Electrolyte Based on Ethylene Carbonate/Ethylene Oxide Random Copolymer. *Macromol. Rapid Commun.* **2017**, *38*, 1600652.
- (44) Tillmann, S. D.; Isken, P.; Lex-Balducci, A. Lithium Coordination in Cyclic-Carbonate-Based Gel Polymer Electrolyte. *J. Phys. Chem. C* 2015, *119*, 14873–14878.
- (45) Johnston, S. F.; Ward, I. M.; Cruickshank, J.; Davies, G. R. Spectroscopic Studies of Triflate Ion Association in Polymer Gel Electrolytes and Their Constituents. *Solid State Ionics* **1996**, *90*, 39–48.
- (46) Schantz, S. On the Ion Association at Low Salt Concentrations in Polymer Electrolytes; a Raman Study of NaCF3SO3 and LiClO4 Dissolved in Poly(Propylene Oxide). *J. Chem. Phys.* **1998**, *94*, 6296.
- (47) Kumar, R.; Sumpter, B. G.; Muthukumar, M. Enhanced Phase Segregation Induced by Dipolar Interactions in Polymer Blends. *Macromolecules* **2014**, 47, 6491–6502.
- (48) Sharick, S.; Koski, J.; Riggleman, R. A.; Winey, K. I. Isolating the Effect of Molecular Weight on Ion Transport of Non-Ionic Diblock Copolymer/Ionic Liquid Mixtures. *Macromolecules* **2016**, 49, 2245–2256.
- (49) Kim, O.; Jo, G.; Park, Y. J.; Kim, S.; Park, M. J. Ion Transport Properties of Self-Assembled Polymer Electrolytes: The Role of Confinement and Interface. *J. Phys. Chem. Lett.* **2013**, *4*, 2111–2117.
- (50) Kuan, W. F.; Remy, R.; Mackay, M. E.; Epps III, T. H. Controlled Ionic Conductivity via Tapered Block Polymer Electrolytes. *RSC Adv.* **2015**, *5*, 12597–12604.